Room-Temperature Strong Coupling between CdSe Nanoplatelets and a Metal-DBR Fabry–Pérot Cavity

Ovishek Morshed,[1] Mitesh Amin,[1] Rob Collison,[1] Nicole MB Cogan,[2] Eric R Koessler,[2] Trevor M Tumiel,[2] William Girten,[2] Farwa Awan,[2] Lele Mathis,[3] Pengfei Huo,[2,1] A Nickolas Vamivakas,[1,4] Teri W Odom,[5,3] and Todd D Krauss[2,1]

[1)]*The Institute of Optics, University of Rochester, Rochester, New York 14627, USA.*
[2)]*Department of Chemistry, University of Rochester, Rochester, New York 14627, USA.*
[3)]*Department of Materials Science and Engineering, Northwestern University, Evanston, Illinois 60208, USA.*
[4)]*Department of Physics and Astronomy, University of Rochester, Rochester, New York 14627, USA.*
[5)]*Department of Chemistry, Northwestern University, Evanston, Illinois 60208, USA.*

(*Electronic mail: todd.krauss@rochester.edu)

(Dated: 21 September 2023)

We present the generation of exciton-polaritons in CdSe nanoplatelets (NPLs) at room temperature in a metal-dielectric hybrid cavity. The optical cavity is packed with NPLs devoid of any spacer, allowing a larger population of emitters to couple to the cavity. The NPL-filled cavity system shows a Rabi splitting of 74.5 meV compared to the previously obtained 41.5 meV Rabi splitting with an NPL-in-PMMA cavity at room temperature. Angle-resolved reflectance and photoluminescence measurements are performed to explore the polariton photophysics by varying the cavity-exciton detuning and temperature. The role of dark states as a reservoir in redistributing polariton populations is also investigated. Mixed quantum-classical dynamics calculations are performed to model the polariton system wherein the theoretical simulations agree with the experimental observations, providing a fundamental understanding of the polariton dynamics within the NPL-cavity hybrid system. These room-temperature exciton-polaritons have the potential to unlock new chemical reaction pathways as well as pave the way for developing cutting-edge quantum technologies.

I. INTRODUCTION

Exciton-polaritons, generated from the strong coupling between electronic states of molecules and photons confined within an optical cavity, have drawn significant interest in polariton chemistry, cavity quantum-electrodynamics, and novel quantum applications[1,2]. These light-matter quasiparticles offer a powerful basis for quantum nonlinear interactions, which are critical for the implementation of complex two-qubit quantum gates and photonic quantum simulations[3–6]. For a practical quantum computer, employing photonic qubit systems offers distinct advantages including preservation of the quantum states of photons due to very weak environmental interaction, maintenance of coherence at room temperature, and compatibility with quantum communication protocols[3,7]. To enable quantum manipulation, quantum information storage and processing, and the creation of ultrafast single-photon switches, it becomes imperative to achieve substantial strong coupling effects in a robust solid-state system that can be actively controlled at room temperature[1,8–10].

The epitaxial growth-based cavity fabrication technique for creating polaritons is not very useful for quantum applications due to being expensive and incompatible with large-scale silicon manufacturing processes as well as detrimental to integrated photonic applications[3]. The prospect of employing colloidal-based exciton-polariton systems for quantum simulation lies in the ability to perform low-cost material synthesis and the potential for room-temperature operation[3,11,12]. Although exciton-polaritons from planar microcavities have shown various intriguing phenomena, such systems are limited by small exciton binding energies and low-temperature operations. Polaritons based on transition metal dichalcogenides (TMDs) have been heavily studied as well due to the strong nonlinear interactions and low effective mass properties from their constituent exciton and photon components. However, the observation of Rabi splitting from such a system also requires cryogenic temperature and the use of sophisticated measurement techniques[13]. Accordingly, there has been an increasing interest in investigating novel systems capable of functioning at room temperature over the last two decades[2]. The observations of Bose-Einstein condensates[11] and strong nonlinearity[14] for colloidal exciton-polaritons at room temperature show the potential of future polariton devices as well as quantum simulators and set a pathway for delving into captivating physics phenomena such as superfluidity and solitons[3].

Exciton-polaritons possess great promise for manipulating various chemical processes[15,16]. The capacity to control the rates of electron transfer processes and chemical reactions in a reversible fashion through light-matter interactions at room temperature holds promise as a means of precisely directing the reactivity of excited states[17]. Strong coupling has been shown to achieve cavity-modified intramolecular electron transfer between different electronic manifolds i.e., singlet fission[18–20], and change chemical reactivity[21,22] as well as reaction-energy landscapes[23]. Electron transfer rates start to become significant when the Rabi splitting from a strongly coupled system reaches around 100 meV[24].

One key challenge in realizing strongly coupled semiconductor systems in ambient conditions is the small binding energy of excitons along with disorder-induced localization effects[13,25]. While incorporating colloidal quantum

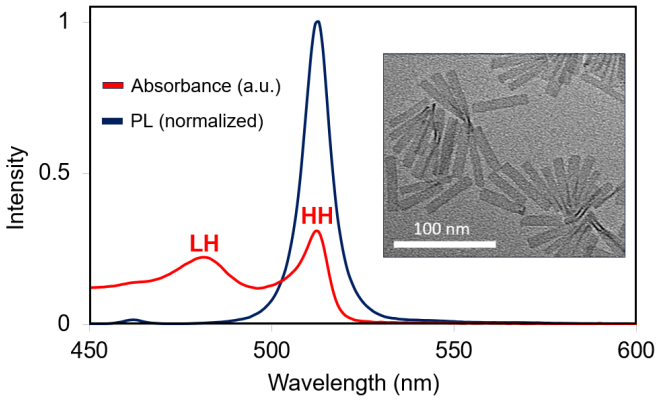

FIG. 1. Absorption and PL spectra of synthesized 4.5 ML CdSe NPL in solution. A TEM image of these NPLs is shown in the inset.

dots (QDs) into the exciton-polariton platform can be challenging due to their broader linewidth, solution-processed nanoplatelets (NPLs) emerge as promising contenders owing to their well-defined thickness minimizing the impact of inhomogeneous size distributions along with high quantum yield and substantial exciton-binding energy[3,26–31]. Much like 2D semiconductor quantum wells, NPLs possess bulk-like attributes in the transverse dimension, while demonstrating quantum confinement in the longitudinal, i.e., thickness direction[32]. As such, these semiconductor NPLs are promising candidates for achieving strong light-matter coupling[31] because of their exceptionally narrow absorption and fluorescence linewidths[30], in-plane transition dipole moment[33] and exceptionally large oscillator strength[34]. To employ a room-temperature based exciton-polariton system, Rabi splitting must exceed the thermal energy of the system[35], a condition which is well-satisfied with CdSe NPLs due to their huge oscillator strength. Incorporating colloidal NPLs into optical cavities poses challenges including complex sample preparation methods[28,36], utilization of plasmonic structures[29,37] with high intrinsic loss and low cooperativity[13] and the use of polymer matrix[31] which limits the number of NPL emitters inside the cavity.

In this work, we introduce a method for integrating concentrated CdSe NPLs into metal-dielectric planar microcavities. This is in contrast to encapsulating the NPLs in a PMMA host matrix that has been done previously to report strong coupling of NPLs in Fabry–Pérot cavities at cryogenic temperature[31]. We use Fourier-space, i.e., angle-resolved optical spectroscopy technique to study the polariton photophysics where the angle information in the far-field projection provides direct insight into the polariton dispersion characteristics[2]. The NPL-cavity system is shown to be in the strong coupling regime with a room-temperature Rabi splitting of 74.5 meV at resonance, confirmed by the angle-resolved reflectance and photoluminescence measurements. The experimental results agree with the quantum dynamics simulations performed to investigate the polariton photophysics in a model Hamiltonian that accounts for cavity loss and phonon-assisted non-adiabatic transitions[31]. Our results show the formation of room-temperature exciton-polaritons in an NPL-filled cavity and pave the way for realizing such a strongly coupled system for polariton chemistry as well as novel quantum applications.

II. SAMPLE FABRICATION

The synthesis of CdSe nanoplatelets (NPLs) was adapted from recently developed procedures[26,38]. The absorption and photoluminescence (PL) spectra of the NPLs are presented in Fig. 1. These NPLs exhibit two well-defined peaks in absorption at 512 nm (2.422 eV) and 481 nm (2.578 eV), corresponding to the heavy-hole and light-hole transitions whereas the emission maximum is at 513 nm (2.417 eV) with a full-width half-maximum (FWHM) of 9.5 nm ($\approx$ 45 meV), resulting in a very small ($\approx$ 5 meV) Stokes shift. The average lateral dimension of the NPLs is estimated from the transmission electron microscope (TEM) image as 38.8 $\pm$ 3.7 nm by 7 $\pm$ 1.1 nm with thickness $\approx$ 1.2 nm, corresponding to a thickness of 4.5 monolayers (MLs).

The cavity is formed by embedding a layer of concentrated 4.5 ML CdSe NPLs in between two highly reflective mirrors. The bottom mirror for this NPL-filled cavity is a distributed Bragg reflector (DBR) and the top mirror is a 40 nm thick metal Ag layer. The NPL film is prepared by drop casting concentrated NPL solutions on top of the DBR substrate, as illustrated in Fig. 2a (more details on fabrication can be found in Appendix B). The fabricated NPL films are very smooth, as shown in Fig. 2b. A schematic of the entire cavity structure is shown in 2c. The quality factor, Q, of the cavity is estimated as $\hbar\omega_c/\gamma_c$ where $\hbar\omega_c$ is the energy of the dummy cavity mode calculated from the central linecut of angle-resolved reflectance of a highly red-detuned cavity with mostly photonic character, the linewidth of which is the cavity decay rate γ_c, leading to a $Q \approx 60$.

III. FORMATION OF EXCITON-POLARITONS

For our planar cavity structure, the cavity-photon field is confined in the z-direction and the energy-momentum relationship of the photon can be expressed as $E_{\rm ph}(\theta) = \frac{\hbar c}{n_e}k = \frac{\hbar c}{n_e}\sqrt{k_\perp^2 + k_\parallel^2}$ where $k_\parallel = \sqrt{k_x^2 + k_y^2}$ represents the in-plane wave vector, $k_\perp$ represents the out-of-plane wavevector in the direction of confined field, c is the speed of the light and n_e is the effective reflective index of the cavity. The relationship between the in-plane and out-of-plane wavevector can be expressed as $\tan\theta = k_\parallel/k_\perp$ where θ corresponds to the angle relative to the z-direction. Accordingly, the cavity photon energy can be expressed as

$$E_{\rm ph}(\theta) = \frac{\hbar c}{n_c}\cdot k_\perp\sqrt{1+\tan^2\theta}, \qquad (1)$$

For small probe angle θ, photon energy can be approximated as

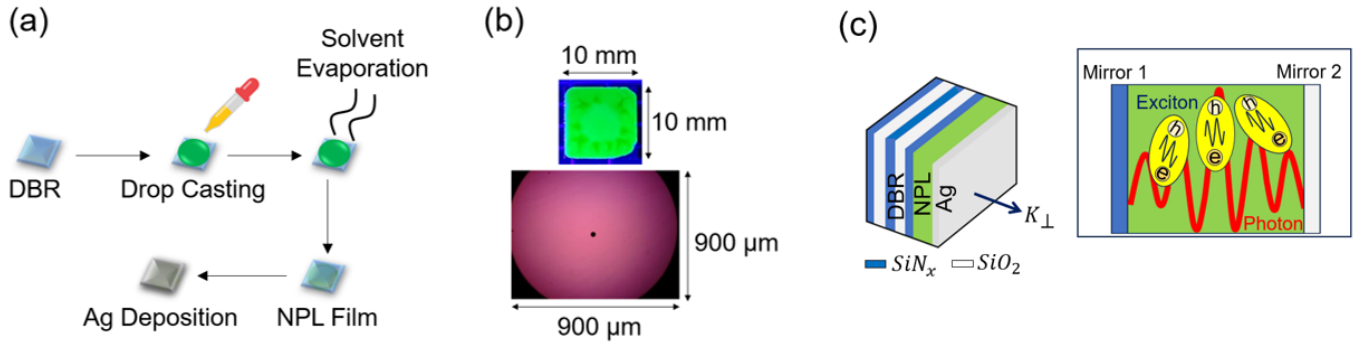

FIG. 2. Schematic of NPL cavity fabrication steps. (a) Solid-state film deposition from NPL colloidal solution to fabricate Fabry–Pérot cavity with a bottom-up approach. (b) Uniform NPL films where the top image corresponds to the deposited film on 10 mm × 10 mm DBR substrate under UV illumination captured with a phone camera and the bottom panel is an optical microscope image on a 900 μm by 900 μm scale, captured with a Filmetrics F20 system. (c) Schematic of the DBR-Metal hybrid cavity structure. The DBR consists of 15.5 pairs of alternating layers of SiN_x and SiO_2, among which only 2.5 pairs are shown in the schematic. The direction of wave propagation, i.e., out-of-plane wavevector is also shown. The interaction between NPL excitonic oscillations and the electromagnetic field of the cavity photons is illustrated in the inset.

$$E_{\rm ph}(\theta) \approx \frac{\hbar c}{n_{\rm c}} \cdot k_\perp (1 + \frac{1}{2}\tan^2\theta) \tag{2}$$

Eq.(2) shows the parabolic dispersion of the cavity photon mode for a small angular range.

In order to model this quantum light-matter system, we consider the Holstein-Tavis-Cummings (HTC) Hamiltonian[39–43]

$$\hat{H} = \hat{H}_{\rm NPL} + \hat{H}_{\rm ph} + \hat{H}_{\rm I} + \hat{H}_{\rm L}, \tag{3}$$

where $\hat{H}_{\rm NPL}$ represents N independent NPLs, $\hat{H}_{\rm ph}$ is the Hamiltonian for the cavity mode, $\hat{H}_{\rm I}$ corresponds to the emitter-photon interactions (between $\hat{H}_{\rm NPL}$ and $\hat{H}_{\rm ph}$), and $\hat{H}_{\rm L}$ describes the interaction between a classical continuous-wave (CW) laser and the NPLs[31].

$\hat{H}_{\rm NPL}$ is modeled as a sum of N identical, non-interacting NPLs where each NPL is modeled as a three-level system,i.e., (i) the ground state $|g_i\rangle$ with the reference electronic energy $E_g = 0$, (ii) the heavy-hole exciton state $|x_i\rangle$ with the energy E_x, and (iii) the high-lying exciton state $|\tilde{x}_i\rangle$ with the energy $E_{\tilde{x}}$ which is in resonance with the pump CW laser driving the NPLs and represents all the high-lying energy states manifold from where the NPLs non-radiatively decay to the heavy-hole exciton state[31]. The model excludes the consideration of the light-hole exciton state due to its decoupling from the initially occupied higher-energy exciton manifold. This decoupling phenomeonon is supported by the absence of PL emission for these light-hole exciton states, as shown in Fig. 1.

The matter-cavity interaction term $\hat{H}_I$ describes the light-matter interaction within the rotating wave approximation (RWA) as

$$\hat{H}_{\rm I} = \sum_i g_{\rm c}\left(\hat{a}_\theta^\dagger |G\rangle\langle X_i| + \hat{a}_\theta |X_i\rangle\langle G|\right), \tag{4}$$

where $\hat{a}_\theta^\dagger$ and $\hat{a}_\theta$ are the photonic creation and annihilation operators associated with the frequency $\frac{\hbar c}{n_{\rm c}} \cdot k_\perp (1 + \frac{1}{2}\tan^2\theta)$, $|G\rangle \equiv |g_1, g_2, ..g_N\rangle$ represents the ground state of N nanoplatelets with the reference electronic energy $E_G = 0$, $|X_i\rangle \equiv |g_1, g_2, ...x_i, ...g_N\rangle$ is the single excited state of the NPLs (where the $i_{\rm th}$ NPL is excited) with energy E_x and $g_{\rm c} = \sqrt{\frac{\hbar\omega_{\rm c}}{2\varepsilon\mathscr{V}}}\hat{\mu}_i \cdot \hat{\mathbf{e}}$ is the matter-cavity coupling strength where $\hat{\mu}_i$ is the transition dipole operator for the $i_{\rm th}$ NPL, ε as the effective permittivity inside the cavity, $\mathscr{V}$ as the quantization volume for the cavity photon field, and $\hat{\mathbf{e}}$ is the polarization direction vector.

In the strong exciton-photon coupling regime, characterized by a coherent energy exchange rate between light and matter that surpasses their decay rate, a phenomenon known as vacuum Rabi splitting occurs, resulting in the creation of two hybrid modes with energies distinct from the original, independent eigenstates[13,44]. Strong coupling is thus characterized by an avoided crossing between the coupled modes and the emergence of two equal-intensity transition peaks at resonance separated by this Rabi splitting[45]. These new eigenmodes resulting from the quantum superposition of excitons and cavity photons, known as the upper polariton (UP) and lower polariton (LP) branches, exhibit a complete admixture of excitonic and photonic properties in the strong coupling regime[46,47]. The energies corresponding to the LP and UP branches can be expressed as

$$\begin{aligned} E_\pm(\theta) = &\frac{1}{2}\left[E_x^0 + \hbar\omega_{\rm c}(1 + \frac{1}{2}\tan^2\theta)\right] \\ &\pm \frac{1}{2}\sqrt{\left[\hbar\omega_{\rm c}(1 + \frac{1}{2}\tan^2\theta) - E_x^0\right]^2 + 4Ng_{\rm c}^2}, \end{aligned} \tag{5}$$

where $\omega_{\rm c} = ck_\perp/n_{\rm c}$ is the frequency of photon in z-direction and $E_X^0 = E_X + \lambda$ is the vertical Franck-Condon exciton energy. The light-matter detuning is defined as

$$\Delta E(\theta) = \hbar\omega_{\rm c}(1 + \frac{1}{2}\tan^2\theta) - E_x^0. \tag{6}$$

For a specific incident angle (θ_0), resonance occurs where

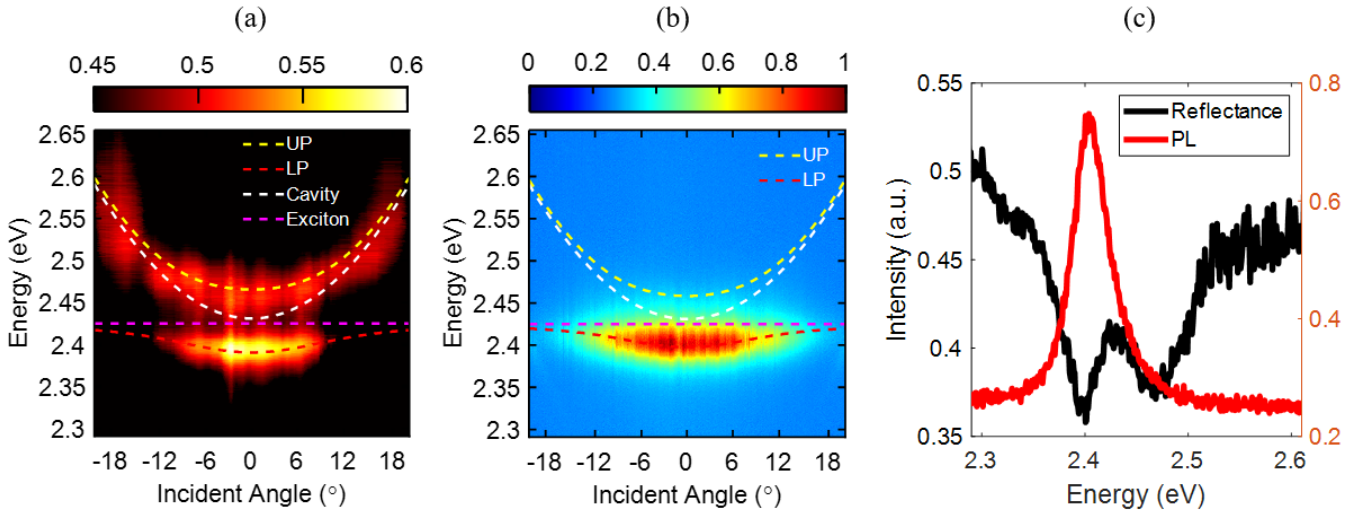

FIG. 3. Angle-resolved measurements of the NPL-cavity hybrid system at T = 295 K. (a) Angle-resolved white light reflectance spectrum (inverted image) showing both the UP and the LP branches. The dashed lines show the exciton, cavity and polariton dispersions fitted using a coupled harmonic oscillator model. (b) Angle-resolved PL spectrum showing only the LP emission where the LP branch flattens at higher angles. (c) Corresponding linecuts of angle-resolved white light reflectance and PL spectra at normal incidence.

the light-matter detuning $\Delta E(\theta_0)$ becomes zero. At resonance. the energy difference between $E_+(\theta_0)$ and $E_-(\theta_0)$ becomes

$$\hbar\Omega_R = E_+(\theta_0) - E_-(\theta_0) = 2\sqrt{N}g_c, \tag{7}$$

This energy difference between the upper and the lower polaritons at resonance is commonly referred to as the vacuum Rabi splitting. It is obvious that the Rabi splitting is proportional to $\sqrt{N}$, *i.e.*, the more NPLs effectively couple to the cavity, the larger Ω_R becomes, which is the motivation of this work. To fulfill the strong coupling criterion, Rabi splitting Ω_R needs to be larger than the combined decay rates of photon (γ_c) and exciton (γ_x).

In general, the energy difference between the two polariton branches can be written as

$$\hbar\Omega_{eff} = \sqrt{[\Delta E(\theta)]^2 + 4Ng_c^2} \tag{8}$$

where $\hbar\Omega_{eff}$ is the effective Rabi splitting which increases with detuning.

IV. EXPERIMENTAL RESULTS

The polaritons formed by the strong coupling of NPLs to the optical cavity are characterized by measuring angle-resolved reflectance and photoluminescence spectra. This measurement is performed using a Fourier space spectroscopy system wherein the back focal plane of the microscope objective is relayed to the entrance slit of the spectrometer through a tube lens, thus transferring the angular information to the spatial coordinates and effectively mapping incident angles into spatial positions. The range of collection angle is calculated to be $\pm$ 20^o from Snell's law. Further information on the experimental setup is available in Appendix C.

Fig. 3a presents the angle-resolved reflectance spectrum for an NPL-filled cavity where the sample is probed by a broadband white light source. It shows two separated branches corresponding to the upper and the lower polariton. As the collection angle increases, the LP branch starts to deviate from the cavity photon dispersion and tends to follow the exciton dispersion characteristics at higher angles, and vice-versa for the UP branch. The two polariton branches can be fitted to $E_+(\theta)$ and $E_-(\theta)$ as expressed in Eq. 5. The fitting parameters are the vertical Franck-Condon exciton energy $E_x^0 = E_x + \lambda$, the photon energy at zero incident angle $E_{ph} = \hbar\omega_c$ and the effective coupling strength $\sqrt{N}g_c$. The collective coupling strength is estimated to be $\sqrt{N}g_c = 37.25$ meV, corresponding to a room temperature Rabi splitting, $\hbar\Omega_R = 74.5$ meV at resonance, i.e. when cavity-exciton detuning, $\Delta E(\theta) = 0$. The Rabi splitting extracted from our NPL-filled cavity system satisfies the strong coupling criterion as

$$\hbar\Omega_R > \sqrt{\gamma_c^2 + \gamma_x^2} = 54.1meV \tag{9}$$

where γ_x is the exciton decay rate, calculated to be 38.2 meV from the FWHM linewidth of single NPL PL spectrum whereas γ_c is the decay rate of cavity photons, calculated to be 38.33 meV from the FWHM linewidth of the central linecut of the reflection spectrum obtained from a dummy red-detuned cavity.

For this particular cavity, the energy of the cavity mode is slightly higher than the exciton mode at normal incidence i.e., at θ = 0^o, resulting in a positively detuned cavity where the UP branch dominates the reflection spectrum across the whole range of collection angle whereas the LP branch loses intensity at higher angles. This zero-angle cavity-exciton detuning is estimated to be $\Delta E = 5.9$ meV. As the collection angle increases, cavity-exciton detuning approaches zero, i.e., the

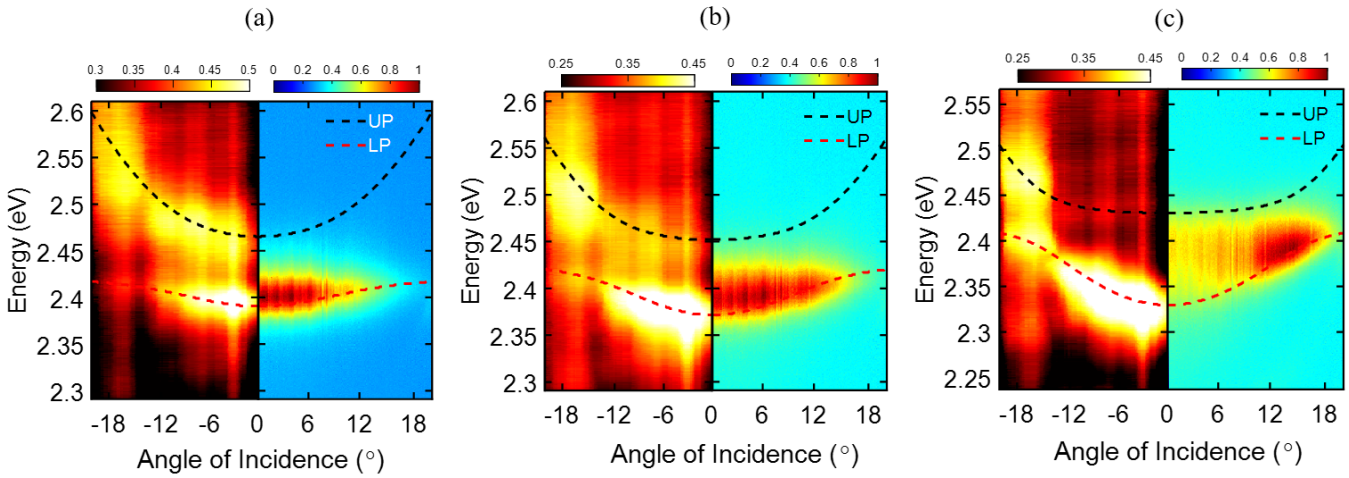

FIG. 4. Angle-resolved measurements for three different cavities with varied detunings at T = 295 K. The left panels of each figure correspond to angle-resolved reflectance spectra whereas the right panels correspond to the PL spectra. The cavity-exciton detunings at normal incidence are (a) ΔE = 5.9 meV, (b) $\Delta E = -$ 36.3 meV and (c) $\Delta E = -$ 79.8 meV. All the three cavities have similar Rabi splitting, $\hbar\Omega_R \approx$ 70-75 meV.

two modes approach resonance[48] and two symmetric equal-intensity reflectivity dips are observed (Fig. 8).

Fig. 3b shows the angle-resolved photoluminescence (PL) measurements at T = 295 K. In this setup, the sample is pumped off-resonantly using a 405 nm continuous wave (CW) diode laser, which facilitates coupling between the ground state and the higher-energy exciton manifold. The PL spectrum clearly demonstrates that polariton emission predominantly occurs within the LP branch. Notably, emission from the UP branch is not observed due to the fast relaxation of the exciton population into the lower-energy states[49]. Fig. 3c complements this by showing corresponding linecuts of the angle-resolved reflectance and PL spectra at normal incidence. The reflectance spectrum reveals two distinct eigenmodes, marked by the presence of two distinguishable dips, while the PL spectrum exhibits a single peak corresponding to only the LP branch.

Fig. 4 shows angle-resolved reflectance and PL measurements for three different cavities with varied detunings at T = 295 K. The value of Rabi splitting doesn't seem to be affected by the variation in detuning since the number of emitters as well as the cavity mode volume hardly changes with a slight change in detuning. However, as detuning increases, i.e., the system deviates from the resonance condition, the phase relationship between the exciton and the cavity mode's oscillations starts to become less favorable for coherent interaction. Nevertheless, the effective Rabi splitting increases with detuning according to Eq. 8. As the cavity mode becomes more and more negatively detuned from the exciton mode, the LP branch tends to have more curvature as it follows the photon dispersion characteristics at small angles, at which, the intensity of the UP branch diminishes in the reflectance spectrum. The width of the LP PL spectrum is larger (almost double) than that of the reflectance spectrum, calculated from the corresponding central linecuts. This arises from vibrational relaxation pathways leading to a broader range of emission energies and defect-induced inhomogeneous broadening. There is also a notable difference between the shape of the reflectance and the emission spectrum for each cavity. The LP emission tends to blue shift compared to the absorption where the broadened PL spectrum overlaps with the uncoupled, i.e., dark exciton emission band.

This blue-shifting phenomenon can be explained by the role of dark states in polariton photophysics. When there is no intermolecular interactions, the polaritons remain decoupled from the exciton modes that do not couple to the cavity, known as the so-called "dark states". However, due to the inherent interactions among molecules, polaritons, which partially encompass molecular degrees of freedom, can interact with these dark states. This interaction between polaritons and dark modes may introduce an additional route for dephasing of polaritons. The rate at which polaritons undergo dephasing is governed by three critical factors: (i) intensity of intermolecular interactions, (ii) molecular weight of the polaritons, and (iii) degree of spectral overlap between the polariton and the dark modes[50].

The dark states, when present in significant numbers, can significantly modify the polariton dispersion characteristics since they have the capacity to draw upon oscillator strength from the bright exciton, resulting from the vibronic coupling and static energy disorder via higher-order processes[17,51]. This happens in the presence of local inhomogeneities, and these intracavity dark states can also borrow photonic character from a bright polariton state owing to coherent local influences[17]. Various sources of inhomogeneity, such as energy disorder, Rabi disorder, and intramolecular vibronic coupling, can lead to interactions between the completely symmetric polariton states and non-symmetric material excitations[17,52–54]. In our NPL-filled cavity system, featuring a significant population of dark exciton states, the observation of blue-shifting of the LP emission is primarily attributed to the redistribution of population away from a symmetric polariton manifold toward the reservoir of dark states[17,49,55]. This occurs as a result of local dissipative

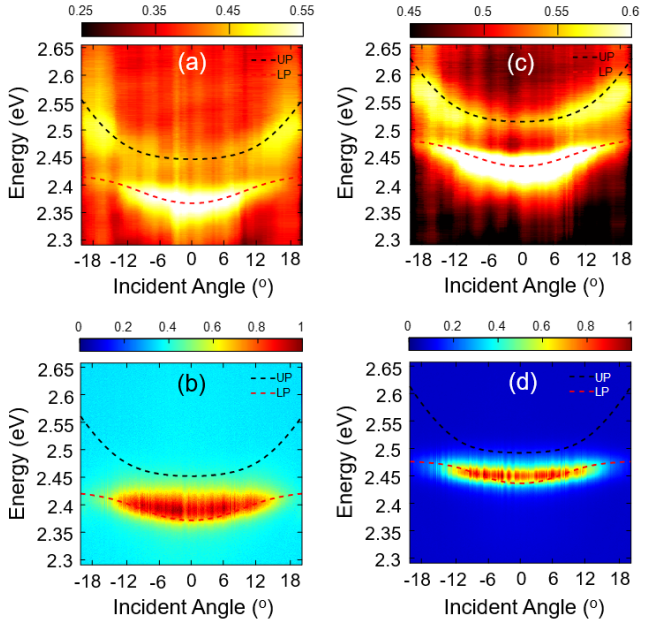

FIG. 5. Temperature-dependent angle-resolved measurements for cavities with similar detuning. The top panel shows the angle-resolved reflection spectrum and the bottom panel represents the angle-resolved PL spectrum. The left and right panels show room temperature (295 K) and low-temperature (5 K) spectra, respectively. (a-b) = − 36.3 meV, $\hbar\Omega_R \approx$ 71.58 meV. (c-d) ΔE = − 31.8 meV, $\hbar\Omega_R \approx$ 74.65 meV.

mechanisms, including non-radiative relaxation and dephasing. These processes ultimately lead to both a blue shift and a broadening of the emission spectrum.

With the increase in detuning, the LP PL intensity also tends to become stronger at higher angles, corresponding to higher in-plane momenta. The observed phenomenon is referred to as the "bottleneck effect", characterized by the accumulation of polaritons within a bottleneck-like region, and reflects a decrease in the exciton-phonon scattering rate at low angles as the lower polaritons descend along their dispersion curve. This reduction in scattering arises from diminished excitonic character, lower density of states resulting from the decrease of polariton effective mass, and increased radiative rates attributable to enhanced photonic character[56]. The combination of these phenomena results in the depletion of the polariton population in the region of lower in-plane momenta with mostly photon-like characteristics[57].

The temperature-dependent characteristics of polariton dispersion have also been examined by measuring angle-resolved spectra of the NPL-cavity system at both room temperature (295 K) and cryogenic temperature (5 K) while maintaining a consistent detuning. It's worth mentioning that spectral measurement obtained from the same spot at different temperatures is not ideal for studying temperature dependence since changes in temperature alter the cavity-exciton detuning. This happens because the absorbance and the PL spectra of these NPLs exhibit a blue-shift at lower temperatures[58]. Additionally, the cavity undergoes a slight reduction in thickness due to the shrinking of the active layer as the temperature goes down. However, the dominant phenomenon influencing the cavity-exciton detuning as temperature decreases is the exciton blue-shift, which tends to create a more negatively detuned cavity at lower temperatures.

Upon fitting the dispersion data, the Rabi splitting is found to be similar during temperature variations, with only a slight increase of approximately 3 meV as the temperature decreases from 295 K to 5 K. This is consistent with the recent observation for 4.5 ML CdSe NPLs that the oscillator strength of their heavy hole excitonic transition is almost constant in the temperature range of 3K – 300 K[34]. Since the oscillator strength does not change, Rabi splitting is not affected by temperature variations as long as the coupling strength exceeds the exciton and photon decay rates. Such a relatively stable Rabi splitting across a range of temperatures removes the need for extreme temperature control and holds significant promise for developing high-performance solid-state devices.

V. CONCLUSION

To summarize, our study demonstrates the achievement of a substantial Rabi splitting in ambient conditions by employing an NPL-filled optical microcavity. The resulting polaritonic hybrid states exhibit a Rabi splitting of 74.5 meV at room temperature. Both the UP and the LP branches can be resolved in the reflectance spectrum whereas the PL spectrum only shows emission from the LP branch due to the fast depletion of the UP state owing to phonon-mediated population relaxation. Rabi splitting, defined as the energy difference between exciton and photon modes at resonance, does not change when detuning is varied, although the change in detuning affects the shape of the polariton dispersion curves. Local disorders and dephasing can significantly alter the population dynamics of the polaritons which can be manifested as a blue-shift of the emission spectrum. The polariton bottleneck effect is also observed with the increase in detuning corresponding to the shift of the cavity mode toward lower energies. The NPL-filled cavity system is found to be temperature robust indicated by a consistent Rabi splitting across a range of temperatures, eliminating the need for sophisticated temperature control. Room-temperature operation of such a polaritonic system offers the feasibility to manipulate chemical reactions and realize real-world quantum applications.

ACKNOWLEDGMENTS

This work was supported by the National Science Foundation Award 2124398 "CCI Phase 1: NSF Center for Quantum Electrodynamics for Selective Transformations (QuEST)" program under Grant number CHE-531223. The authors also acknowledge the support from Cornell Nanoscale Science and Technology Facility (CNF) and Intergated Nanosystems Center (URnano) for their nanofabrication facilities.

DATA AVAILABILITY STATEMENT

The data that support the findings of this study are available from the corresponding author upon reasonable request.

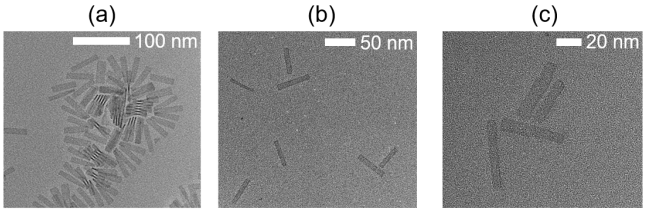

FIG. 6. TEM Images of synthesized 4.5 ML CdSe NPL.

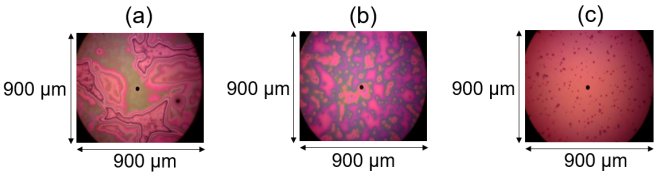

FIG. 7. Microscope images of NPL films with various deposition methods. (a) Drop-casted NPL film without the removal of excess ligands, indicating a wet film with phase separation between the solvent and the ligand. (b) Spin-coated NPL film without the removal of excess ligands, showing a rough and wet film. (c) Spin-coated NPL film from NPL-PMMA mixture, resulting in aggregates. The dimension of all the images is 900 μm by 900 μm.

Appendix A: Synthesis

1. Chemicals

Cadmium acetate dihydrate ($Cd(OAc)_2.2H_2O$) (98%), cadmium nitrate tetrahydrate (98%), sodium myristate ($\geq$99%), selenium powder ($\geq$99.5%), technical grade 1-octadecene (ODE), and technical grade oleic acid (OA) are purchased from Sigma-Aldrich. N-hexane and methanol are purchased from Fisher Chemical.

2. Preparation of Cadmium Myristate

3 grams of cadmium nitrate tetrahydrate is first dissolved in 200 mL methanol. In a separate beaker, 5 grams of sodium myristate is dissolved in 500 mL of methanol using vigorous stirring. The solution containing the cadmium nitrate tetrahydrate is then added dropwise to the sodium myristate and stirred for 2 hours. The cloudy white suspension is vacuum filtered to obtain the cadmium myristate powder which is washed with excess methanol. The obtained powder is dried under vacuum overnight and stored in a glovebox for future use.

3. Synthesis of 4.5 ML CdSe NPLs?

4.5 monolayer thick CdSe nanoplatelets are prepared by combining 180 mg of dried cadmium myristate and 30 mg of selenium powder in 15 mL of ODE within a 100 mL three-necked round-bottom flask. The solution is degassed under vacuum at 120^0 for 1 hour. The mixture is returned to nitrogen flow and the temperature was set to 240^0. At 210^0, 100 mg of cadmium acetate dihydrate is immediately added into the reaction mixture. Once at 240^0, the temperature is held constant for 8 minutes and then immediately cooled to 170^0 using an air gun and placed in a water bath. At 160^0, 2 mL of OA is injected and the temperature is allowed to decrease to room temperature. Once the mixture reaches room temperature, 15 mL of hexane is injected, and centrifuged at 3000 rpm for 10 minutes. The supernatant containing the ODE and quantum dots is discarded and the pellet containing the NPLs is redispersed in 12 mL of hexane and allowed to sit for at least one hour before centrifuging at 6000 rpm for 10 minutes. The supernatant containing the NPLs is kept and stored in the dark under ambient conditions for further use.

Appendix B: Sample Preparation

1. Removal of Excess Ligands

To remove excess oleic acid ligands from the as-synthesized NPL solutions, ethanol is added to the stock solution until turbid ($\approx$1:1, EtOH:NPL) and then centrifuged at 6000 rpm for 15 minutes. The pellet containing the NPLs is then resuspended in hexane and washed once more with ethanol followed by the resuspension in hexane to produce an orangish solution of washed 4.5 ML NPLs.

2. NPL Film and Cavity Fabrication

The DBR, forming the bottom mirror of the cavity, is fabricated through plasma-enhanced chemical vapor deposition of 31 alternating layers of SiN_x ($SiH_4/NH_3/N_2$ gas) and SiO_2 (SiH_4/N_2O gas) on top of a silicon substrate. The DBR substrates are cleaned using acetone, isopropyl alcohol and deionized water before depositing the NPLs on top of them. The NPL film is prepared by drop casting 16 μL of purified and concentrated NPL solutions (150–200 mg/mL) on top of the DBR and covered with a beaker to slow down the evaporation of the solvent. After a couple of minutes, a solid film of NPL is obtained on the DBR substrate. A 40 nm thick silver (Ag) layer is then grown on top of it through physical vapor deposition (PVD) to complete the cavity fabrication.

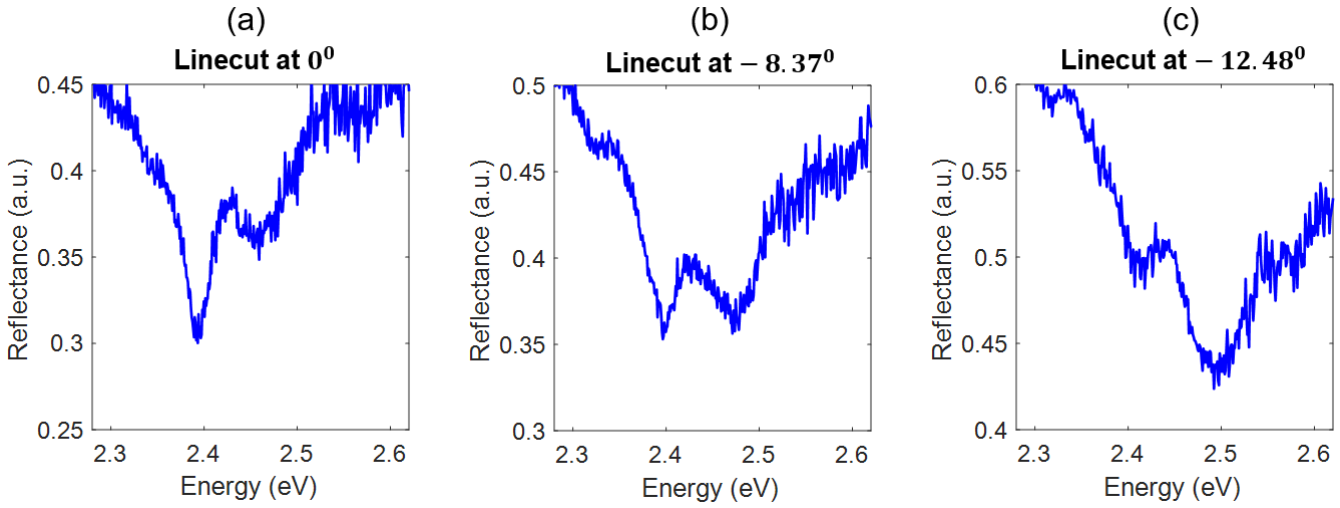

FIG. 8. Vertical linecuts of angle-resolved reflectance spectrum shown in Fig. 3(a). The linecut shows two symmetric modes corresponding to the LP and the UP branches when the exciton mode is in resonance with the cavity mode (b). As the cavity moves away from resonance, the modes become asymmetric where either the LP branch (a) or the UP branch (c) possesses higher intensity, characterized by the reflectance dips.

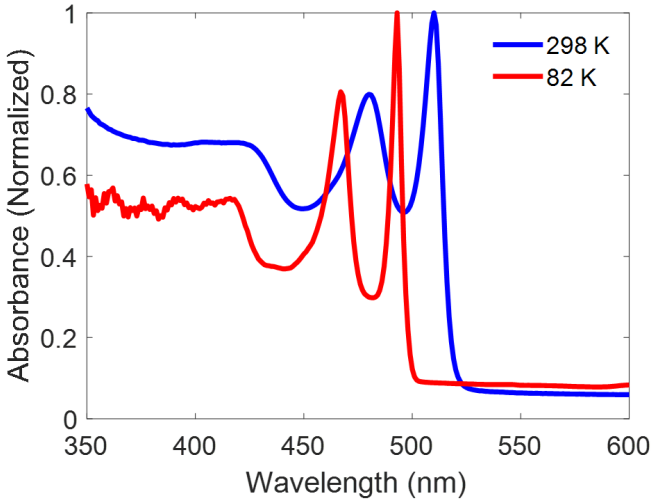

FIG. 9. Absorbance spectra of CdSe NPL Films at two different temperatures.

Appendix C: Optical Characterization

1. Absorption and Emission Measurements of NPL Colloidal Solutions

Absorption and emission measurements are performed with a quartz cuvette that has a path length of 1 cm. Absorbance spectra are collected using a PerkinElmer Lambda 950 UV/Vis/NIR spectrophotometer, while photoluminescence (PL) characterization is conducted using a modular fluorometer system (Acton Research) equipped with a photomultiplier tube (PMT) detector.

2. TEM Measurements

TEM samples are spotted on lacey carbon grids with 300 mesh copper support. TEM micrographs are recorded using a FEI Tecnai F20 field emission microscope with a 200 kV accelerating voltage. The NPL dimensions are determined by measuring 12 individual NPLs on the TEM images.

3. Thin Film Measurements

The Filmetrics F20 system is used to analyze the film quality and measure the thickness of the NPL films. For this measurement, the sample is illuminated with a tungsten-halogen white light source with an operating range from 400 nm to 3000 nm where the reflected light is captured and fed back to the spectrometer input port via another fiber optic cable.

4. Angle-Resolved Measurements

Angle-resolved reflection and PL measurements are performed at room temperature (295 K) and low temperature (5 K) by placing the sample within a compressed-He cooled cryostation (Montana Instruments) with a 0.5 mm thick fused SiO_2 optical window and equipped with an XYZ-piezo translator (Attocube). A Fourier-space spectroscopy system with a two-dimensional (2D) charge-coupled device (CCD) detector (Teledyne Princeton Instruments PyLon, 1340 $\times$ 1300 pixels) is used to resolve the collected light by angle of reflection or emission along one axis of the detector (the axis parallel to the spectrometer's entry slit) while simultaneously resolving the collected light by wavelength along the axis perpendicular to the entrance slit. Light reflected or emitted from the sample

is collected by an infinity-corrected objective (Nikon S Plan Flour, 60X, 0.7 NA, correction collar set to 0.5 mm), giving a $\pm 44^0$ collection angle range in free space (with 0^0 corresponding to light emitted or reflected along the surface normal). The Fourier image plane of the sample, located at the back focal plane of the objective, is directed toward the entrance slit of a spectrometer (Teledyne Princeton Instruments SP2750i). This is achieved by employing a tube lens to create a Fourier image plane in free space, which is then relayed onto the entrance slit using two additional relay lenses.

Reflection spectra are measured using a white LED (Thorlabs) source where the reflected light from the sample is coupled into an optical fiber and imaged into the spectrometer. To remove the spectrum of the light source from the measured sample spectra, the raw angle-resolved reflection spectra from the sample are divided by the "flat field" spectrum, i.e., the angle-resolved reflection spectrum of a silver film (200 nm of Ag deposited by electron beam evaporation onto a 2 nm Ge wetting layer on a Si chip, coated with 15 nm SiO_2 to prevent corrosion). The same collection path is used for PL measurements where a 405 nm CW diode laser non-resonantly excites the system with 500 μW power incident on the back of the microscope objective. For both PL and WL reflection spectra measurements, a 450 nm long-pass filter is used in the collection path to remove the reflected light from the source and an exposure time of 60 s is used for all measurements.

IV. REFERENCES

[1] J. Wen, H. Wang, W. Wang, Z. Deng, C. Zhuang, Y. Zhang, F. Liu, J. She, J. Chen, H. Chen, *et al.*, "Room-temperature strong light–matter interaction with active control in single plasmonic nanorod coupled with two-dimensional atomic crystals," Nano letters **17**, 4689–4697 (2017).

[2] S. Ghosh, R. Su, J. Zhao, A. Fieramosca, J. Wu, T. Li, Q. Zhang, F. Li, Z. Chen, T. Liew, *et al.*, "Microcavity exciton polaritons at room temperature," Photonics Insights **1**, R04–R04 (2022).

[3] Y. Chen, D. Sharp, A. Saxena, H. Nguyen, B. M. Cossairt, and A. Majumdar, "Integrated quantum nanophotonics with solution-processed materials," Advanced Quantum Technologies **5**, 2100078 (2022).

[4] D. E. Chang, V. Vuletić, and M. D. Lukin, "Quantum nonlinear optics—photon by photon," Nature Photonics **8**, 685–694 (2014).

[5] L.-M. Duan and H. Kimble, "Scalable photonic quantum computation through cavity-assisted interactions," Physical review letters **92**, 127902 (2004).

[6] I. Carusotto and C. Ciuti, "Quantum fluids of light," Reviews of Modern Physics **85**, 299 (2013).

[7] J. L. O'brien, A. Furusawa, and J. Vučković, "Photonic quantum technologies," Nature Photonics **3**, 687–695 (2009).

[8] D. Sanvitto and S. Kéna-Cohen, "The road towards polaritonic devices," Nature materials **15**, 1061–1073 (2016).

[9] T. Volz, A. Reinhard, M. Winger, A. Badolato, K. J. Hennessy, E. L. Hu, and A. Imamoğlu, "Ultrafast all-optical switching by single photons," Nature Photonics **6**, 605–609 (2012).

[10] W. Chen, K. M. Beck, R. Bücker, M. Gullans, M. D. Lukin, H. Tanji-Suzuki, and V. Vuletić, "All-optical switch and transistor gated by one stored photon," Science **341**, 768–770 (2013).

[11] R. Su, J. Wang, J. Zhao, J. Xing, W. Zhao, C. Diederichs, T. C. Liew, and Q. Xiong, "Room temperature long-range coherent exciton polariton condensate flow in lead halide perovskites," Science advances **4**, eaau0244 (2018).

[12] R. Su, S. Ghosh, J. Wang, S. Liu, C. Diederichs, T. C. Liew, and Q. Xiong, "Observation of exciton polariton condensation in a perovskite lattice at room temperature," Nature Physics **16**, 301–306 (2020).

[13] B. Li, S. Zu, Z. Zhang, L. Zheng, Q. Jiang, B. Du, Y. Luo, Y. Gong, Y. Zhang, F. Lin, *et al.*, "Large rabi splitting obtained in ag-ws2 strong-coupling heterostructure with optical microcavity at room temperature," Opto-Electronic Advances **2**, 190008 (2019).

[14] J. Wu, S. Ghosh, R. Su, A. Fieramosca, T. C. Liew, and Q. Xiong, "Nonlinear parametric scattering of exciton polaritons in perovskite microcavities," Nano Letters **21**, 3120–3126 (2021).

[15] S. Pannir-Sivajothi, J. A. Campos-Gonzalez-Angulo, L. A. Martínez-Martínez, S. Sinha, and J. Yuen-Zhou, "Driving chemical reactions with polariton condensates," Nature communications **13**, 1645 (2022).

[16] B. M. Weight, T. D. Krauss, and P. Huo, "Investigating molecular exciton polaritons using ab initio cavity quantum electrodynamics," The Journal of Physical Chemistry Letters **14**, 5901–5913 (2023).

[17] F. Herrera and J. Owrutsky, "Molecular polaritons for controlling chemistry with quantum optics," The Journal of chemical physics **152** (2020).

[18] E. Eizner, L. A. Martínez-Martínez, J. Yuen-Zhou, and S. Kéna-Cohen, "Inverting singlet and triplet excited states using strong light-matter coupling," Science Advances **5**, eaax4482 (2019).

[19] S. Takahashi, K. Watanabe, and Y. Matsumoto, "Singlet fission of amorphous rubrene modulated by polariton formation," The Journal of Chemical Physics **151** (2019).

[20] K. Stranius, M. Hertzog, and K. Börjesson, "Selective manipulation of electronically excited states through strong light–matter interactions," Nature Communications **9**, 2273 (2018).

[21] A. Thomas, J. George, A. Shalabney, M. Dryzhakov, S. J. Varma, J. Moran, T. Chervy, X. Zhong, E. Devaux, C. Genet, *et al.*, "Ground-state chemical reactivity under vibrational coupling to the vacuum electromagnetic field," Angewandte Chemie **128**, 11634–11638 (2016).

[22] M. E. Mondal, E. R. Koessler, J. Provazza, A. N. Vamivakas, S. T. Cundiff, T. D. Krauss, and P. Huo, "Quantum dynamics simulations of the 2d spectroscopy for exciton polaritons," The Journal of Chemical Physics **159** (2023).

[23] J. A. Hutchison, T. Schwartz, C. Genet, E. Devaux, and T. W. Ebbesen, "Modifying chemical landscapes by coupling to vacuum fields," Angewandte Chemie International Edition **51**, 1592–1596 (2012).

[24] A. Mandal, T. D. Krauss, and P. Huo, "Polariton-mediated electron transfer via cavity quantum electrodynamics," The Journal of Physical Chemistry B **124**, 6321–6340 (2020).

[25] V. M. Agranovich, M. Litinskaia, and D. G. Lidzey, "Cavity polaritons in microcavities containing disordered organic semiconductors," Physical Review B **67**, 085311 (2003).

[26] S. Ithurria and B. Dubertret, "Quasi 2d colloidal cdse platelets with thicknesses controlled at the atomic level," Journal of the American Chemical Society **130**, 16504–16505 (2008).

[27] S. Ithurria, M. Tessier, B. Mahler, R. Lobo, B. Dubertret, and A. L. Efros, "Colloidal nanoplatelets with two-dimensional electronic structure," Nat. Mater. **10**, 936–941 (2011).

[28] L. C. Flatten, S. Christodoulou, R. K. Patel, A. Buccheri, D. M. Coles, B. P. Reid, R. A. Taylor, I. Moreels, and J. M. Smith, "Strong exciton–photon coupling with colloidal nanoplatelets in an open microcavity," Nano Letters **16**, 7137–7141 (2016).

[29] J. M. Winkler, F. T. Rabouw, A. A. Rossinelli, S. V. Jayanti, K. M. McPeak, D. K. Kim, B. Le Feber, F. Prins, and D. J. Norris, "Room-temperature strong coupling of cdse nanoplatelets and plasmonic hole arrays," Nano letters **19**, 108–115 (2018).

[30] M. D. Tessier, C. Javaux, I. Maksimovic, V. Loriette, and B. Dubertret, "Spectroscopy of single cdse nanoplatelets," ACS nano **6**, 6751–6758 (2012).

[31] L. Qiu, A. Mandal, O. Morshed, M. T. Meidenbauer, W. Girten, P. Huo, A. N. Vamivakas, and T. D. Krauss, "Molecular polaritons generated from strong coupling between cdse nanoplatelets and a dielectric optical cavity," The Journal of Physical Chemistry Letters **12**, 5030–5038 (2021).

[32] M. L. Steigerwald and L. E. Brus, "Semiconductor crystallites: A class of large molecules," Acc. Chem. Res. **23**, 183–188 (1990).

[33] Y. Gao, M. C. Weidman, and W. A. Tisdale, "Cdse nanoplatelet films with controlled orientation of their transition dipole moment," Nano Letters **17**, 3837–3843 (2017).

[34]B. T. Diroll and R. D. Schaller, "Reexamination of the giant oscillator strength effect in cdse nanoplatelets," The Journal of Physical Chemistry C **127**, 4601–4608 (2023).
[35]A. Pawlis, A. Khartchenko, O. Husberg, D. J. As, K. Lischka, and D. Schikora, "Large room temperature rabi-splitting in ii–vi semiconductor microcavity quantum structures," Microelectronics journal **34**, 439–442 (2003).
[36]M. Oda, K. Yamato, J. Egashira, and H. Kondo, "Room-temperature strong coupling of hexane-dispersed colloidal cdse nanoplatelets in a microcavity composed of two bragg reflectors," arXiv preprint arXiv:2309.04743 (2023).
[37]I. Shlesinger, H. Monin, J. Moreau, J.-P. Hugonin, M. Dufour, S. Ithurria, B. Vest, and J.-J. Greffet, "Strong coupling of nanoplatelets and surface plasmons on a gold surface," ACS Photonics **6**, 2643–2648 (2019).
[38]A. A. Rossinelli, A. Riedinger, P. Marqués-Gallego, P. N. Knüsel, F. V. Antolinez, and D. J. Norris, "High-temperature growth of thick-shell cdse/cds core/shell nanoplatelets," Chemical communications **53**, 9938–9941 (2017).
[39]J. Keeling and S. Kena-Cohen, "Bose–einstein condensation of exciton-polaritons in organic microcavities," Annu. Rev. Phys. Chem. **71**, 435–459 (2020).
[40]F. Herrera and F. C. Spano, "Absorption and photoluminescence in organic cavity qed," Phys. Rev. A **95**, 053867 (2017).
[41]F. Herrera and F. C. Spano, "Dark vibronic polaritons and the spectroscopy of organic microcavities," Phys. Rev. Lett. **118**, 223601 (2017).
[42]J. Feist, J. Galego, and F. J. Garcia-Vidal, "Polaritonic chemistry with organic molecules," ACS Photonics **5**, 205–216 (2018).
[43]K. B. Arnardottir, A. J. Moilanen, A. Strashko, P. Törmä, and J. Keeling, "Multimode organic polariton lasing," Phys. Rev. Lett. **125**, 233603 (2020).
[44]P. Törmä and W. L. Barnes, "Strong coupling between surface plasmon polaritons and emitters: a review," Reports on Progress in Physics **78**, 013901 (2014).
[45]D. G. Lidzey, D. Bradley, M. Skolnick, T. Virgili, S. Walker, and D. Whittaker, "Strong exciton–photon coupling in an organic semiconductor microcavity," Nature **395**, 53–55 (1998).
[46]V. Savona, "Fifteen years of microcavity polaritons," The Physics of Semiconductor Microcavities (2007).
[47]W. Chiang, O. Morshed, and T. Krauss, *Quantum Confined Semiconductor Nanocrystals* (American Chemical Society, 2023).
[48]D. Lidzey, D. Bradley, T. Virgili, A. Armitage, M. Skolnick, and S. Walker, "Room temperature polariton emission from strongly coupled organic semiconductor microcavities," Physical review letters **82**, 3316 (1999).
[49]R. Bhuyan, J. Mony, O. Kotov, G. W. Castellanos, J. Gomez Rivas, T. O. Shegai, and K. Borjesson, "The rise and current status of polaritonic photochemistry and photophysics," Chemical Reviews (2023).
[50]T. E. Li, A. Nitzan, and J. E. Subotnik, "Polariton relaxation under vibrational strong coupling: Comparing cavity molecular dynamics simulations against fermi's golden rule rate," The Journal of Chemical Physics **156** (2022).
[51]F. C. Spano, "The spectral signatures of frenkel polarons in h-and j-aggregates," Accounts of chemical research **43**, 429–439 (2010).
[52]C. López, H. Christ, J. Retamal, and E. Solano, "Effective quantum dynamics of interacting systems with inhomogeneous coupling," Physical Review A **75**, 033818 (2007).
[53]F. Spano, "Optical microcavities enhance the exciton coherence length and eliminate vibronic coupling in j-aggregates," The Journal of Chemical Physics **142** (2015).
[54]F. Herrera and F. C. Spano, "Cavity-controlled chemistry in molecular ensembles," Physical Review Letters **116**, 238301 (2016).
[55]N. Shammah, N. Lambert, F. Nori, and S. De Liberato, "Superradiance with local phase-breaking effects," Physical Review A **96**, 023863 (2017).
[56]M. Laitz, A. E. Kaplan, J. Deschamps, U. Barotov, A. H. Proppe, I. García-Benito, A. Osherov, G. Grancini, D. W. deQuilettes, K. A. Nelson, *et al.*, "Uncovering temperature-dependent exciton-polariton relaxation mechanisms in hybrid organic-inorganic perovskites," Nature Communications **14**, 2426 (2023).
[57]F. Tassone, C. Piermarocchi, V. Savona, A. Quattropani, and P. Schwendimann, "Bottleneck effects in the relaxation and photoluminescence of microcavity polaritons," Physical Review B **56**, 7554 (1997).
[58]A. F. Vong, S. Irgen-Gioro, Y. Wu, and E. A. Weiss, "Origin of low temperature trion emission in cdse nanoplatelets," Nano letters **21**, 10040–10046 (2021).